ETHIOPIAN JOURNAL OF TEXTILE AND APPAREL

EiTEX

ETHIOPIAN INSTITUTE OF TEXTILE AND FASHION TECHNOLOGY
BAHIR DAR UNIVERSITY,
ETHIOPIA

DYNAMIC PERFORMANCE ASSESSMENT OF SINGLE-GLAZED AND DOUBLE-GLAZED SOLAR AIR HEATER SYSTEMS FOR TEXTILE INDUSTRY

Tamene Adisu Hailu[1*]

[1]Lecturer, Madda Walabu University, Mechanical Engineering, Robe, Ethiopia

[2]PhD Candidate, Adama Science and Technology University, Thermal Engineering, Adama, Ethiopia

ISSN: (Print) (Online) Journal homepage: https://journals.bdu.edu.et/index.php/ejta

To cite this article: Tamene Adisu Hailu (2026), DYNAMIC PERFORMANCE ASSESSMENT OF SINGLE-GLAZED AND DOUBLE-GLAZED SOLAR AIR HEATER SYSTEMS FOR TEXTILE INDUSTRY, 17-30

DYNAMIC PERFORMANCE ASSESSMENT OF SINGLE-GLAZED AND DOUBLE-GLAZED SOLAR AIR HEATER SYSTEMS FOR TEXTILE INDUSTRY

Tamene Adisu Hailu[1*]

[1]Lecturer, Madda Walabu University, Mechanical Engineering, Robe, Ethiopia

[2]PhD Candidate, Adama Science and Technology University, Thermal Engineering, Adama, Ethiopia

[*]Corresponding Author:

Email: tamene.adisu@astu.edu.et

ABSTRACT

The textile industry requires considerable thermal energy, particularly for low-temperature drying and finishing operations. Conventional heating methods, commonly powered by fossil fuels, contribute to rising energy costs. Though, a solar air heater (SAH) stands out as a simple, affordable, and eco-friendly device that transforms solar radiation into thermal energy. It can be effectively utilized for space heating, crop drying, and industrial heating. SAHs utilize radiation, convection, and conduction heat transfer mechanisms. Minimizing conduction losses through insulation and better glazing is crucial. As such, a transient analysis was performed for flat-plate SAHs for the weather conditions of Adama City. It was found that the single-glass SAH shows a definite diurnal and seasonal pattern, with air temperatures reaching a maximum of 82.34°C in February and maintaining effective heating above 60°C between 10:00 and 14:00 for most months. In contrast, the double-glass SAH achieves air temperatures of up to 90.57°C in February, with prolonged retention of above 80°C between 10:00 and 14:00 for most months. As a whole, both configurations absorb solar energy efficiently, but double-glass SAH remains thermally superior to its single-glass counterpart in every working condition. Hence, the integration of SAHs into textile drying operations presents a sustainable and cost-effective alternative for supplying low-temperature thermal energy.

Keywords: Low-Temperature Drying, Renewable Energy, Solar Air Heater, Thermal Performance.

1. INTRODUCTION

The textile manufacturing industry represents a key segment within the global manufacturing industries that convert fibers into clothing by undergoing various processes, as seen from Figure 1 (Catarino, Sampaio and Gonçalves, 2025). Some of these processes include fiber preparation, spinning, forming fabrics, wet processing, and making clothing. The energy requirement for wet processing like washing, scouring, bleaching, dyeing, and drying are considerable amounts of heat (40-110°C) (Farhana et al., 2022). Traditionally, heat is supplied by burning coal, oil, or natural gas. Such sources pose problems of costliness, unreliable supply, and release greenhouse gases (Čerdancova et al., 2021). As such, alternative method to fulfill thermal energy requirements becomes necessary. This can be provided by renewable energy like solar thermal, bioenergy, biogas, and geothermal (P. Kumar et al., 2022).

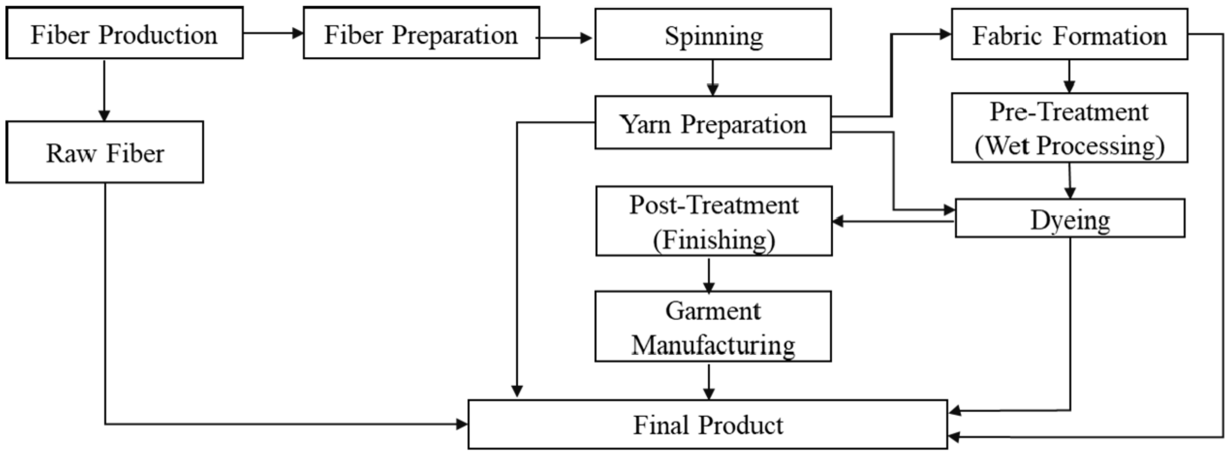

Figure 1: Overview of textile sector processes

Abbreviation and Nomenclatures

A_C	*Collector area*	I_{sc}	*Solar constant*	V_w	*Wind velocity*
C_p	*Specific heat*	I_T	*Tilted surface irradiance*	α	*Absorptivity of plate*
d_e	*Edge insulation height*	k	*Thermal conductivity*	α_a	*Thermal diffusivity of air*
F_d	*Dust factor*	L	*Length of absorber*	β	*Surface slope angle*
F_s	*Shading factor*	m	*Mass*	β_1	*Coefficient of expansion*
g	*Gravitational constant*	Nu	*Nusselt number*	δ	*Declination angle*
h	*Convection coefficient*	$\bar{n}_s$	*Average sunshine hour*	ε	*Emissivity*
$\bar{H}$	*Daily global radiation*	Q	*Total heat*	θ	*Angle of incidence*
$\bar{H}_b$	*Daily beam radiation*	R_a	*Rayleigh number*	θ_z	*Zenith angle*
$\bar{H}_d$	*Daily diffuse radiation*	R_b	*Geometric factor*	ϕ	*Latitude of the location*
$\bar{H}_o$	*Extraterestrial radiation*	Re	*Reynolds number*	μ_a	*Air dynamic viscosity*
$\bar{I}$	*Hourly global radiation*	t	*Time*	ρ	*Density, Ground albedo*
$\bar{I}_b$	*Hourly beam radiation*	T	*Temperature*	τ	*Transmissivity of glass*
$\bar{I}_d$	*Hourly diffuse radiation*	v	*Kinematic viscosity*	σ	*Stefan-Boltzman constant*

Solar air heater (SAH) converts solar radiation into thermal energy to heat air (Duffie and Beckman, 2013). SAHs represent simple, cheap, and green solutions for varying applications: industrial process heating, crop drying, and space heating (Singh *et al.*, 2022). Their excellency to advance sustainable technologies is manifested by the SAHs that can satisfy a broad spectrum of needs and enhance efficiency while assuring less dependence on conventional energy (Srivastava and Rai, 2017).

SAH consists of an absorber plate-an essentially black surface-for the absorption of solar radiation and heat transfer to the air flowing over it (Ashja *et al.*, 2025). Located above the absorber plate is the glazing, a transparent glass which facilitates the entrance of solar radiation through it but inhibits convection losses, thus forming a kind of greenhouse heat-trapping effect inside (Ansari and Nassab, 2022). The space between the glazing and the absorber plate becomes the air channel in which the air is heated as it passes through the system (Farzan, Mahmoudi and Zaim, 2023).

The concept behind SAH is to capture solar radiation through the glass cover, which is transferred to an absorber plate (Farzan, Mahmoudi and Zaim, 2023). The energy absorbed heats the plate, and subsequently heats air that flows across the plate (Ansari and Nassab, 2022). Thus, the efficiency of SAH systems depends on the performance and balancing of heat gain by using the absorptive materials and heat loss mechanisms (Haldia *et al.*, 2024). These SAHs can be classified by the mode of operation, i.e., active or passive, the absorber plate used (Nemati, 2024), whether porous or nonporous, and the number of glazing layers from unglazed to double-glazed (Shandal, Abed and Al-Shamkhee, 2020).

Variations in absorber plates exist with respect to material that may be metal or nonmetal, or some composite, and the shape could be flat, finned, or ribbed (Kumar *et al.*, 2024). In nonporous class, the air flows along the top, or along the bottom, or along both sides of the absorber plates, but never through it, with configurations below or along both sides giving better heat retention and efficiency (Al-Chlaihawi, Alyas and Badr, 2023). The porous-type plates contain small holes through which air is forced to flow through enhancing heat transfer and providing an environmentally and economically viable heating system (Saboohi *et al.*, 2023). Through selective coatings, glazing, and innovative airflow design, the efficiency of SAH can be maximized by manipulating the natural mechanisms of heat transfer (Ameri, Farzan and Nobari, 2021).

Consequently, this paper mainly deals with the transient thermal performance of the SAH in the specific weather conditions of Adama City, Ethiopia. The study begins with predicting hourly solar radiation incident on a tilted surface based on sunshine hour data to accurately simulate the availability of solar energy in the study area. The study then develops a transient thermal model to represent the operation of a single-glazed flat plate SAH using this solar energy potential data. A transient thermal analysis of a double-glazed configuration is also modeled in the same way to compare the two designs mentioned above. In essence, this study describes the transient thermal performance of SAH, providing information regarding the transient behavior of glass cover, absorber plate and outlet air temperature under local weather conditions.

2. LITERATURE REVIEW

The textile industry involves very complicated production process that starts from fiber production and ends at the manufacture of the garment (Khude, 2017). Among all processes involved, wet processing such as dyeing and finishing plays the most important role in adding value to the textiles by giving them color, softness, and durability (Catarino, Sampaio and Gonçalves, 2025). Nevertheless, due to its complications, the industry consumes huge amounts of energy. In this regard, fiber preparation usually accounts for 21%, spinning for 11-18%, and weaving for 23% of the energy needed to produce textiles from fibers to the end product (Farhana *et al.*, 2022). Energy costs in a textile mill account for 15-20% of total production costs and become the second largest cost after the raw material cost (Khude, 2017).

Thermal energy is essential mainly for wet processing such as pre-treatment, dyeing, printing, and washing (Leseeka, 2024). The thermal process consumes high amounts of energy, up to 40% of the total thermal energy in the factory (Patel *et al.*, 2021). Conventional methods of thermal energy production involve the use of steam boilers or burners fueled by coal to generate steam at high temperatures needed for the above operations (Leseeka, 2024). The textile industry uses large quantities of water in its operations; therefore, its overall energy consumption is proportional to the amount of water consumed (Patel *et al.*, 2021).

Several important textile operations, on the other hand, demand low temperature heating that is generally considered below 100°C (Ramaiah and Shekar, 2018). These include processes such as washing (40-80°C), mercerization (60-70°C), and dark washing or enzyme treatment (50°C) (L. Kumar *et al.*, 2022). Moreover, pre-heating of boiler feedwater, which is needed in almost all industries, works at 30-100°C (Leseeka, 2024). Hot water generation, as opposed to steam generation, becomes more relevant with the lower temperatures and is an excellent way of utilizing thermal energy (Tasmin *et al.*, 2022).

Industrial processes like scouring require a temperature range of 90-110°C, whereas bleaching requires a temperature range of 60-100°C (Ramaiah and Shekar, 2018). Stenter machines, which are employed for drying fabrics, usually function in a range of 100°C to 200°C, and these are the most energy-intensive processes (Farhana *et al.*, 2022). Steam is needed at a temperature range of 120°C to 180°C for the proper conduct of such processes (P. Kumar *et al.*, 2022).

Supplying the heat from traditional energy sources such as fossil fuels, including coal, oil, and natural gas, involves a number of major negative consequences on the environment (Patel *et al.*, 2021). Industrial processes account for about 10% of total greenhouse gas emissions worldwide; the use of fossil fuels to provide heat for industrial purposes is one of their major contributors (Leseeka, 2024). Industrial processes across the globe have led to emission of 9.0 gigatons of CO_2 in the year 2022 alone (Catarino, Sampaio and

Gonçalves, 2025). Constraints relating to economics and operations have also prevented further dependency on fossil fuel. This type of fuel is characterized by high prices, limited supplies, and expensive maintenance (Leseeka, 2024). In traditional boiler technology, there are energy losses, such that for the U.S. textile industry, on-site losses of profile and boiler are 8% and 7%, respectively (Khude, 2017).

Solar thermal energy has huge potential to offer the low temperature heat needed in the textile industry, especially for operations below 95°C (P. Kumar *et al.*, 2022). The most economically viable technology in this regard is the use of flat plate collector (L. Kumar *et al.*, 2022). These systems are commercially established, easy to maintain, and capable of attaining up to 89% solar fraction efficiency (Leseeka, 2024). Incorporation of such technologies in the system can be highly effective in reducing the carbon footprint of an organization. For example, the reduction in CO_2 emissions from production of one ton of yarn is 382.5 tons (P. Kumar *et al.*, 2022).

2. METHODOLOGY

The transient thermal analysis of flat SAHs in the specific weather of Adama city, is the main focus of this paper. The study starts with the prediction of hourly solar radiation incident on a tilted surface using sunshine hour data. Then, the study develops a transient thermal model for the operation of a single-glazed flat plate SAH using this solar potential data. The behavior of a double-glazed layout is examined using a similar methodology, enabling a comparison of the two designs. The analysis takes into account how the temperatures of the absorber, glass, and air outlet change over time.

3.1. Solar Energy Potential of Adama

Adama city is located at 8.54°N 39.27°E, in Oromia region, Ethiopia. It is located at an elevation of 1,712 meters; it lies 99 kilometers southeast of Addis Ababa. The city is positioned between the great rift valley to the east and the base of an escarpment to the west (Adama City Admninistration, 2025). As shown in Table 1, the city has high solar energy potential with average sunshine hour ($\bar{n}s$) exceeding 8 hours per day for ten months of the year. Only during two months of the summer, July and August, the average sunshine hour is below 8 hours, with July showing low average recorded sunshine hour of 6.8 hour.

Table 1: Sunshine hour (Venkatachalam, Samuel and Solomon, 2019), and Maximum Temperature (Tmax) and Minimum Temperature (Tmin) of Adama city (Climate Data, 2024)

Month	Jan	Feb	Mar	Apr	May	Jun	Jul	Aug	Sep	Oct	Nov	Dec
$\bar{n}_s$	9.3	10.2	9.0	8.6	8.0	8.2	6.8	7.9	8.2	8.8	10.0	9.2
Tmax (^{O}C)	26.2	28.0	28.7	28.9	29.1	28.5	26.8	26.1	26.8	26.8	26.0	25.3
Tmin (^{O}C)	12.4	13.7	15.5	16.7	16.5	15.8	15.7	15.3	15.2	15.3	13.6	12.1

3.1.1. Monthly Average Daily Radiation

Prediction of the solar potential of Adama city can be started using the sun shine hours, shown in Table 1, and average day of the month (n) and representative day of the month (N_{rep}), provided on Table 2.

Table 2: Average and representative days of months (Duffie and Beckman, 2013)

Month	Jan	Feb	Mar	Apr	May	Jun	Jul	Aug	Sep	Oct	Nov	Dec
N_{rep}	17	16	16	15	15	11	17	16	15	15	14	10
n	17	47	75	105	135	162	198	228	258	288	318	344

As such, the declination angle (δ) is determined from Cooper equation as shown in equation (1) as cited in (Duffie and Beckman, 2013):

$$\delta = 23.45 \sin\left(360 \frac{284 + n}{365}\right) \quad (1)$$

Where δ is the declination angle, and n is the number of the day.

Similarly, the sunset hour angle is determined:

$$\omega_s = cos^{-1}(-\tan\phi \tan\delta) \quad (2)$$

Test

Where ωs is the sunset hour angle, ϕ is the latitude, and δ is the declination angle
Then, monthly mean extraterrestrial radiation ($\bar{H}o$) on a horizontal surface, can be obtained by the Klein relationship as discussed in (Duffie and Beckman, 2013), as shown in equation (3).

$$\bar{H}_o = \frac{24 * 3600\ I_{sc}}{\pi}\left(1 + 0.033\cos\left(\frac{360n}{365}\right)\right)\left(\cos\phi\cos\delta\sin\omega_s + \frac{\pi\omega_s}{180}\sin\phi\sin\delta\right) \quad (3)$$

Where $\bar{H}o$ is monthly average extraterrestrial radiation on a horizontal surface, Isc is the solar constant, n is the number of the day, ϕ is the latitude, δ is the declination angle, and ωs is the sunset hour angle.

Moreover, monthly mean of the maximum possible daily hours of bright sunshine ($\bar{Ns}$) is determined from Cooper's formula (Ansari and Nassab, 2022), as shown in equation (4):

$$\bar{N}_s = \frac{2}{15}\omega_s \quad (4)$$

Where $\bar{Ns}$ is monthly average of the maximum possible daily hours of bright sunshine, and ωs is the sunset hour angle

Then, the regression parameters (a) and (b) used in modified Angstrom equation of regression (Singh et al., 2022), can be determined from equation (5).

$$a = -0.110 + 0.323\left(\frac{\bar{n}_s}{\bar{N}_s}\right) + 0.235\cos\phi \quad (5)$$

$$b = -0.694\left(\frac{\bar{n}_s}{\bar{N}_s}\right) - 0.533\cos\phi + 1.449$$

Where a and b are empirical constants obtained through regression, ϕ is the latitude, $\bar{ns}$ is monthly average daily hours of bright sunshine, and $\bar{Ns}$ is monthly average of the maximum possible daily hours of bright sunshine.
Then, using modified Angstrom equation of regression, monthly average daily global radiation ($\bar{H}$) can be found as discussed in (Duffie and Beckman, 2013), as shown in equation (6).

$$\bar{H} = \bar{H}_O\left(a + b\frac{\bar{n}_s}{\bar{N}_s}\right) \quad (6)$$

Where $\bar{H}$ is monthly average daily global radiation on horizontal surface, $\bar{HO}$ is monthly average extraterrestrial radiation for the same location, a and b are empirical constants obtained through regression, $\bar{ns}$ is monthly average daily hours of bright sunshine, and $\bar{Ns}$ is monthly average of the maximum possible daily hours of bright sunshine.

Similarly, monthly average daily diffuse radiation ($\bar{H}d$) can be found as shown in equation (7) (Ansari and Nassab, 2022).

$$\bar{H}_d = \bar{H}\left(0.931 - 0.814\frac{\bar{n}_s}{\bar{N}_s}\right) \quad (7)$$

Where $\bar{Hd}$ is monthly average diffuse radiation, $\bar{H}$ is monthly average daily global radiation on horizontal surface, $\bar{ns}$ is monthly average daily hours of bright sunshine, and $\bar{Ns}$ is monthly average of the maximum possible daily hours of bright sunshine.

Moreover, monthly mean daily beam radiation ($\bar{H}b$) is determined as shown in equation (8) (Ansari and Nassab, 2022).

$$\bar{H}_b = \bar{H} - \bar{H}_d \quad (8)$$

is monthly average beam radiation, $\bar{H}$ is monthly average daily global radiation on horizontal surface, and $\bar{Hd}$ is monthly average diffuse radiation.

3.1.2. Monthly Mean Hourly Radiation

Prediction of monthly mean hourly radiation starts with determining regression coefficients (a') and (b') using equation (9) (Duffie and Beckman, 2013).

$$a' = 0.409 + 0.5016\sin(\bar{\omega}_s - 60) \quad (9)$$

$$b' = 0.6609 - 0.4767\sin(\bar{\omega}_s - 60)$$

Where a and b are empirical constants obtained through regression, and $\bar{\omega s}$ is monthly average sunset hour.

Then, monthly mean hourly global radiation ($\bar{I}$) can be calculated as shown in equation (10) (Nemati, 2024).

$$\bar{I} = \bar{H}\left(\frac{\pi}{24}(a + b\cos\bar{\omega})\frac{\cos\bar{\omega} - \cos\bar{\omega}_s}{\sin\bar{\omega}_s - \frac{\pi}{180}\bar{\omega}_s\cos\bar{\omega}_s}\right) \quad (10)$$

Where $\bar{I}$ is monthly average hourly global radiation on horizontal surface, $\bar{H}$ is monthly average daily global radiation on horizontal surface, a and b are empirical constants obtained through regression, and $\bar{\omega s}$ is monthly average sunset hour.

Moreover, monthly mean hourly diffuse radiation ($\bar{I}d$) can be found from equation (11) (Farzan, Mahmoudi and Zaim, 2023).

$$\bar{I}_d = \bar{H}_d\left(\frac{\pi}{24}\frac{\cos\bar{\omega}-\cos\bar{\omega}_s}{\sin\bar{\omega}_s-\frac{\pi}{180}\bar{\omega}_s\cos\bar{\omega}_s}\right) \quad (11)$$

Where $\bar{I}_d$ is monthly average hourly diffuse radiation on horizontal surface, $\bar{H_d}$ is monthly average daily diffuse radiation on horizontal surface, and $\bar{\omega s}$ is monthly average sunset hour.

Furthermore, monthly average hourly beam radiation ($\bar{I}_b$) can be found from equation (12) (Nemati, 2024).

$$\bar{I}_b = \bar{I} - \bar{I}_d \quad (12)$$

Where $\bar{I}_b$ is monthly average hourly beam radiation on horizontal surface, $\bar{I}$ is monthly average hourly global radiation on horizontal surface, and $\bar{I}_d$ is monthly average hourly diffuse radiation on horizontal surface.

3.1.3. Solar Radiation on a Tilted Surface

The geometric factor (Rb), can be determined from equation (13), and solar radiation on a tilted surface (IT) can be determined from equation (14) (Singh et al., 2022).

$$R_b = \frac{\cos\theta}{\cos\theta_Z} = \frac{\sin(\phi-\beta)\sin\delta+\cos(\phi-\beta)\cos\delta\cos\omega}{\sin\phi\sin\delta+\cos\phi\cos\delta\cos\omega} \quad (13)$$

$$I_T = I_bR_b + 0.5I_d(1+\cos\beta) + 0.5\rho(I_b+I_d)(1-\cos\beta) \quad (14)$$

Where R_b is the geometric factor, θ is the angle of incidence, θ_Z is the zenith angle, ϕ is the latitude, β is the surface slope angle δ is the declination angle, ω is the hour angle, I_T is the total hourly irradiance on a tilted surface, I_b is the hourly beam irradiance, I_d is the hourly diffuse irradiance, and ρ is the ground albedo.

3.1.4. Hourly Ambient air temperature

Using the daily maximum ($Tmax$) and daily minimum temperatures ($Tmin$) given in Table 1, based on the sinusoidal variation, the hourly variation of ambient air temperatures ($Tamb(t)$) can be predicted from, as shown in equation (15) (Nemati, 2024).

$$T_{amb}(t) = T_{max} - \frac{T_{max}-T_{min}}{2}\left(1-sin\left(\frac{t\pi-9\pi}{12}\right)\right) \quad (15)$$

Where $T(t)$ is the ambient temperature at any time t, T_{max} is the mean daily maximum temperature, T_{min} is the mean daily minimum temperature, and t is the time in hour.

3.2. Transient Analysis

To develop a transient analysis of the SAH, the heat balance equations for the absorber plate, glass cover, and the air inside the collector is considered. As such, one-dimensional heat transfer, and uniform temperature within each component, are assumed. The rate of change of energy stored in the absorber plate, outer glass cover, inner glass cover, and air stream, and convection coefficient for the enclosed space ($hC{,}P{-}g$) are given by equations 16, 17, 18, 19, and 20, respectively.

$$\left(mC_p\right)_P\frac{dT_{Pd}}{dt} = [0.95(\tau\alpha)A_cI_T] - \left[A_C\sigma\frac{\left((T_{Pd}+273)^4-\left(T_{gdi}+273\right)^4\right)}{\left(\frac{1}{\varepsilon_P}+\frac{1}{\varepsilon_g}-1\right)}\right] - \left[A_Ch_{C,P-g}\left(T_{Pd}-T_{gdi}\right)\right] - \left[A_Ch_{C,P-a}(T_{Pd}-T_{ad})\right] - \left[A_C\frac{k_i}{\delta_B}(T_{Pd}-T_\infty)\right] - \left[2(W+L)l\frac{k_i}{\delta_E}(T_{Pd}-T_\infty)\right] \quad (16)$$

$$(mC_p)_g \frac{dT_{gdo}}{dt} = [A_c I_T \tau(1-\tau)] + [A_C h_{C,P-g}(T_{gdi} - T_{gdo})] - [A_C h_w(T_{gdo} - T_\infty)] - [A_C \varepsilon_g \sigma((T_{gdo}+273)^4 - (T_{sky}+273)^4)] + \left[A_C \sigma \frac{\left((T_{gdi}+273)^4 - (T_{gdo}+273)^4\right)}{\left(\frac{1}{\varepsilon_g} + \frac{1}{\varepsilon_g} - 1\right)}\right] \quad (17)$$

$$(mC_p)_g \frac{dT_{gdi}}{dt} = [A_c I_T(1-\tau)] + [A_C h_{C,P-g}(T_{Pd} - T_{gdi})] - [A_C h_w(T_{gdi} - T_{gdo})] - [A_C \varepsilon_g \sigma((T_{gdi}+273)^4 - (T_{sky}+273)^4)] + \left[A_C \sigma \frac{\left((T_{Pd}+273)^4 - (T_{gdi}+273)^4\right)}{\left(\frac{1}{\varepsilon_P} + \frac{1}{\varepsilon_g} - 1\right)}\right] \quad (18)$$

$$(mC_p)_a \frac{dT_{ad}}{dt} = [A_C h_{C,P-a}(T_{Pd} - T_{ad})] - \left[\frac{(mC_p)_a}{\Delta\tau}(T_{ad,o} - T_{ad,i})\right] \quad (19)$$

$$h_{C,P-g} = \frac{k_a}{l}\left\{1 + 1.44\left[1 - \frac{1708\sin(1.8\beta)^{1.6}}{R_{a\cos\beta}}\right]\left[1 - \frac{1708}{R_{a\cos\beta}}\right]^+ + \left[\left(\frac{R_{a\cos\beta}}{5830}\right)^{1/3} - 1\right]^+\right\} \quad (20)$$

Where (mC_p), I_T, τ, α, A_C, σ, L, l, W, and h_w, are mass*specific. heat, hourly irradiance on a tilted surface, transmissivity, absorptivity, collector area, Stefan Boltzmann's constant, length of the absorber plate, height of insulation, width of the absorber plate, and wind convection coefficient, respectively. T_{Pd}, T_{gdi}, T_{gdo}, T_∞, T_{ad}, $T_{a,}$, $T_{a,o}$, and T_{sky}, are temperature of absorber plate, inner glass cover, outer glass cover, ambient air, air stream, inlet air, outlet air, and sky, respectively. ε_P and ε_g are the emmisivity of plate and glass, respectively. $h_{C,-g}$ and $h_{C,P-a}$, are convection coefficient of enclosed space, and air, respectively. k_i and k_a, are thermal conductivity of insulation, and air, respectively. δ_B and δ_E, are thickness of back insulation, and edge insulation, respectively.

Similarly, using Dittus-Boelter equation as cited in (Duffie and Beckman, 2013), convective heat transfer coefficient ($h_{C,-a}$) used in equations (16) and (19), can be determined from:

$$h_{C,P-a} = 0.023 Re^{0.8} Pr^{0.4} \frac{k_a}{L} \quad (21)$$

Where $h_{C,-a}$ is the convection coefficient for the air, R_e is the Reynolds number, P_r is the Prandtl number of the air, k_a is the thermal conductivity of air, and L is the length of the absorber plate.

Moreover, the convection heat transfer between ambient air and the glass cover depends on the velocity of the ambient air. As such, according to (Duffie and Beckman, 2013), wind convection coefficient (hw) used in equation (17), can be determined from:

$$h_w = 5.7 + 3.8V_w \quad (22)$$

Where h_w is the wind convection coefficient, and V_w is the wind velocity.

The design parameters shown in Table 3 are used for the transient analysis of SAH.

Table 3: Design parameters of Solar Air Heater

Parameter	Value	Parameter	Value	Pa
A_C	2 m^2	L	2m	
β	15 degrees	δ_e	0.03m	
ε_p	0.10	ε_g	0.88	
V_w	2.5m/s	ρ	0.2	

4. RESULTS AND DISCUSSION

The transient thermal analysis of single and double glass solar air heaters is conducted for the specific weather of Adama city. For each model, the analysis takes into account how the temperatures of the absorber, glass, and air outlet change over time. Hence, the results obtained from both models will be discussed here. In addition, the comparison of both models is performed.

4.1. Solar Energy Potential of Adama

Figure 2 illustrates the hourly trends of global, diffuse and beam solar radiation of Adama city, throughout the month and year. All radiation types peaking around midday and declining symmetrically in the morning and afternoon. Global radiation peaks from February to April, reaching 3.5 MJ/m²/hour, and then decline to reach its lowest point in July at 3.0 MJ/m²/hour. Beam radiation closely follows the global trend but with slightly lower peaks, indicating its dependence on clear skies. The beam radiation peaks at 2.75 MJ/m²/hour in February, due to clearer skies and higher solar angles. Then, decline reaching its lowest point of 1.7 MJ/m²/hour in July, coinciding with the rainy season and increased cloud cover. Conversely, diffuse radiation remains relatively low, with more pronounced contributions during overcast conditions, particularly noticeable in July and August. It starts peaking during the wet season in July, 1.35 MJ/m²/hour, and decreasing as clearer skies return. Hence, optimal months for solar energy generation in Adama City are February to May, when global and beam radiation are highest.

Moreover, Figure 2 presents the diurnal and seasonal solar radiation patterns on a tilted surface in Adama city. As such, the highest values of radiation occur in February (3.55 MJ/m²/hour). Whereas, July has the lowest peak (2.91 MJ/m²/hour) likely due to rainy-season cloud cover. The radiation follows a symmetrical bell curve, rising sharply from 6:00–7:00, peaking at noon, and declining gradually until 18:00. This indicates that, Adama's strong solar potential is evident, with irradiance greater than 3 MJ/m²/hour for 4-5 hours daily (10:00–14:00) in most months.

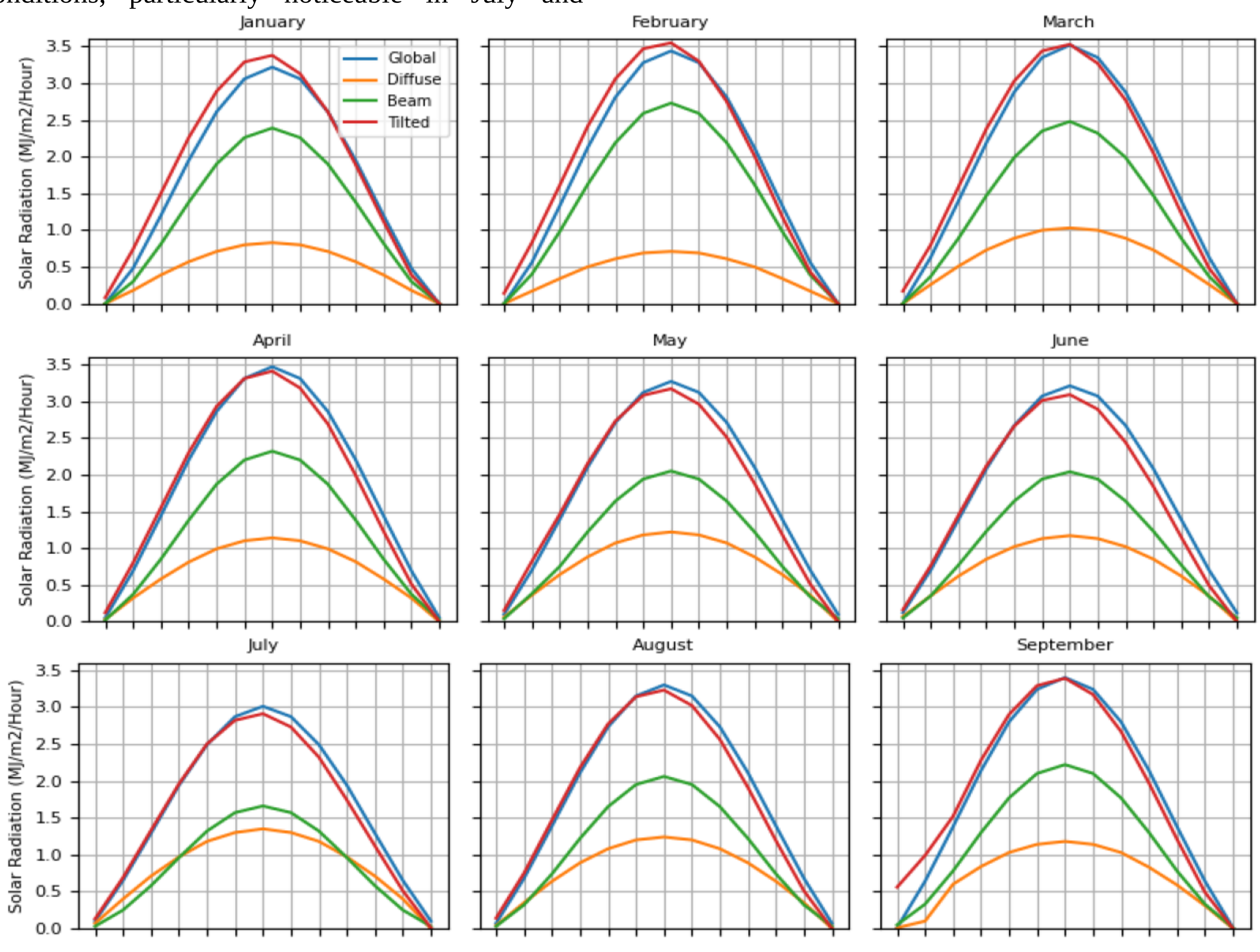

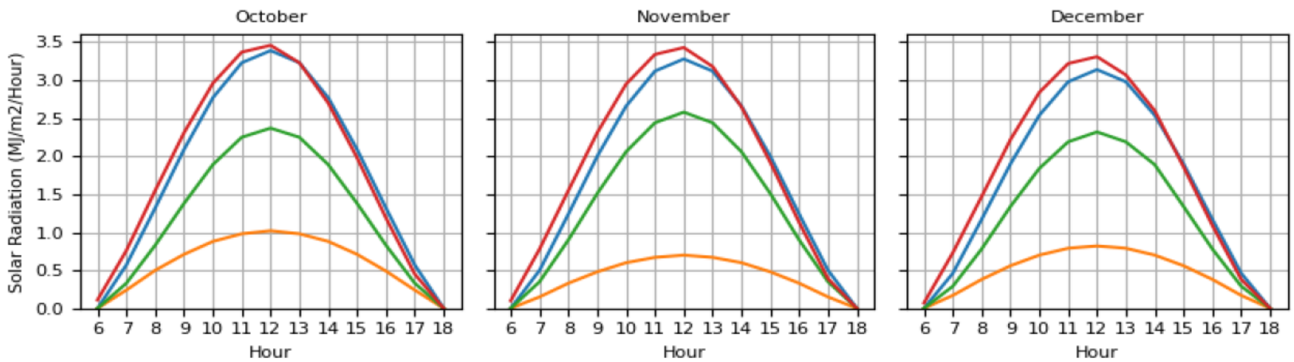

Figure 2: Monthly average hourly solar radiation of Adama City

4.2 Performance of Absorber Plate

Figure 3 demonstrates superior transient performance of double-glass SAH compared to single-glass systems, with the absorber plate consistently achieving higher temperatures across all months due to enhanced insulation from the additional glass layer. The absorber of a single-glass SAH peaks at 125.1°C in February around midday. Similarly, the double-glass solar air heater achieves significantly high absorber temperatures, peaking at 139.8°C in February around midday. The double-glass configuration maintains elevated temperatures often 10°C higher. These results show how the second glass layer minimizes heat loss, enabling more efficient solar energy utilization year-round.

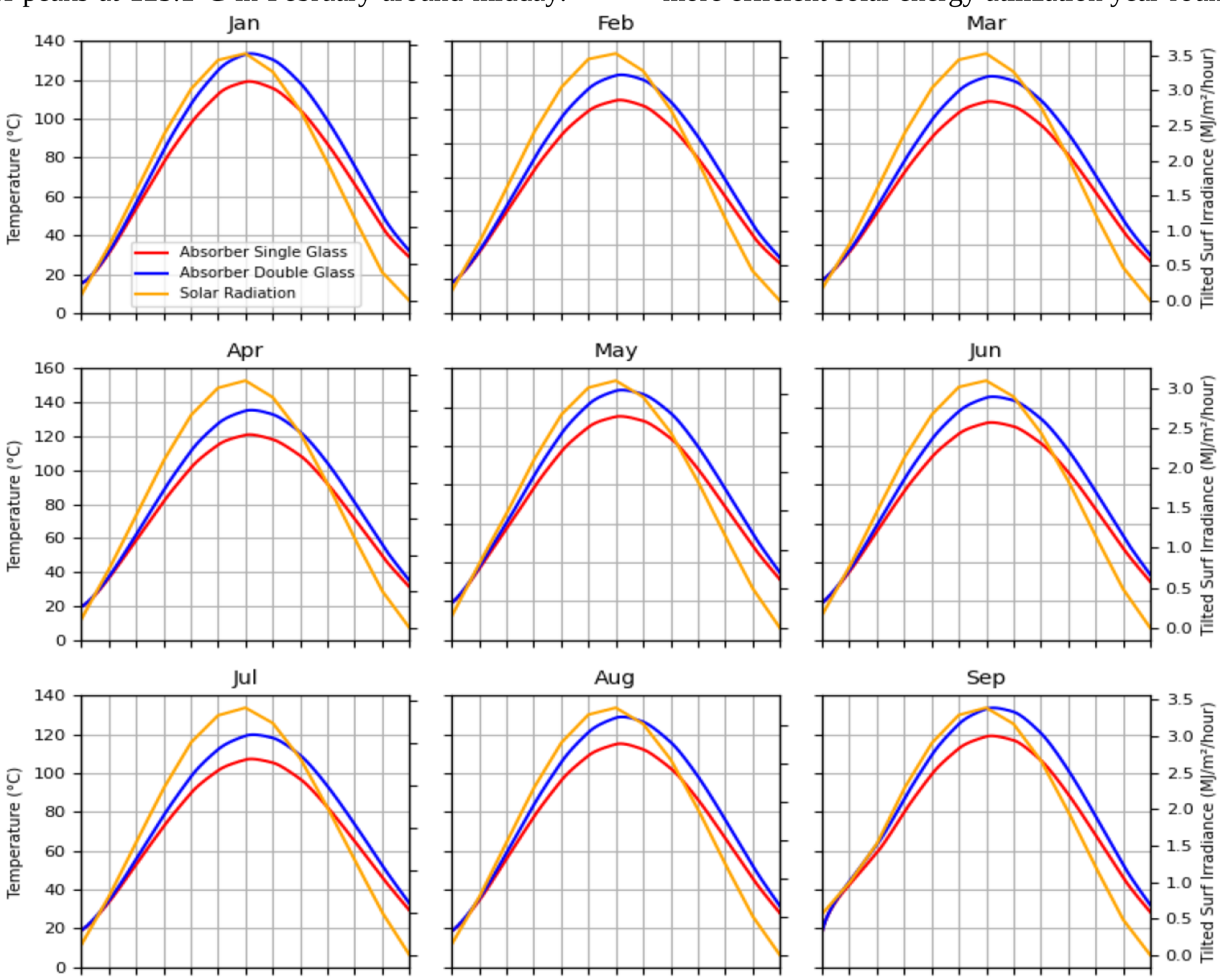

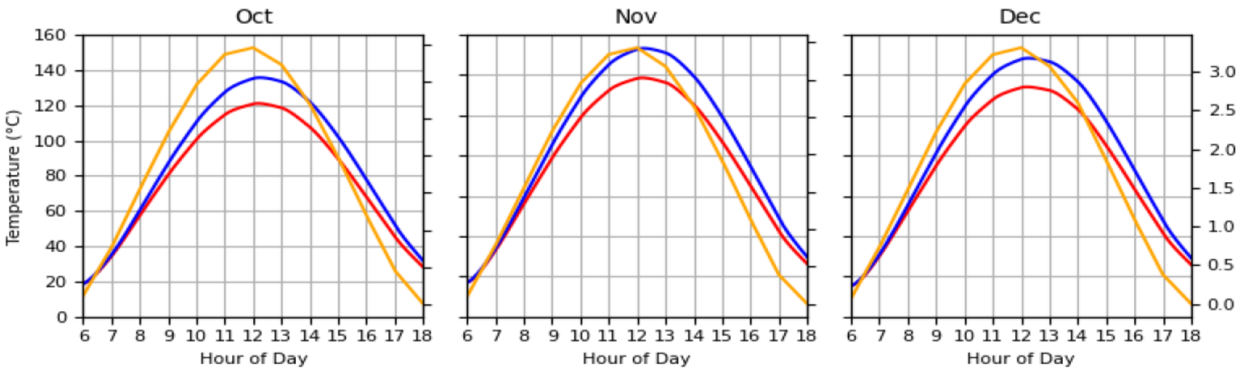

Figure 3: Comparison of absorber plate temperature of single and double glass SAH

4.3. Performance of Glass Cover

Figure 4 demonstrates superior thermal performance of double-glass SAH compared to single-glass systems, with the inner glass cover consistently maintaining higher temperatures, with maximum values reaching 81.61°C in February. In addition, the outer glass temperature peaks around midday exceeding 40°C in most months, with maximum values of 45.0°C in February. Whereas, the single glass cover temperature peak around midday, with the highest values reaching 48°C in February. The temperature of inner glass cover maintains significantly elevated temperatures often 20-30°C higher than that of single glass cover.

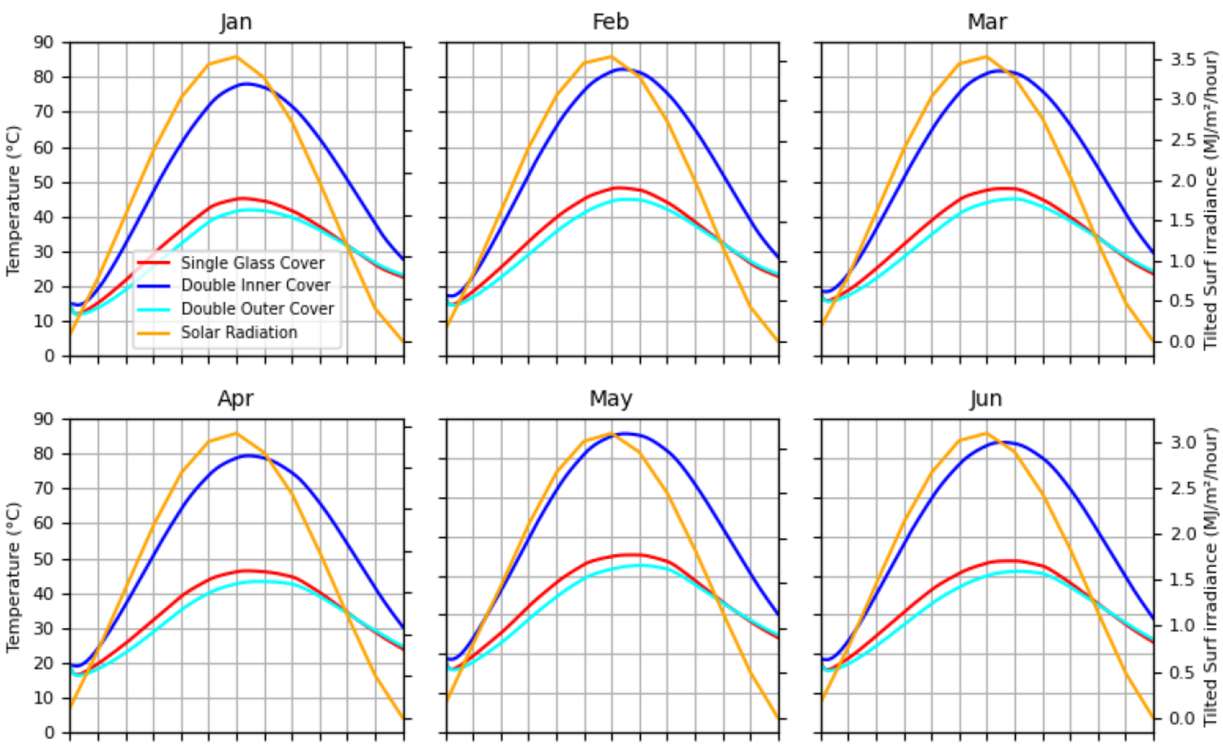

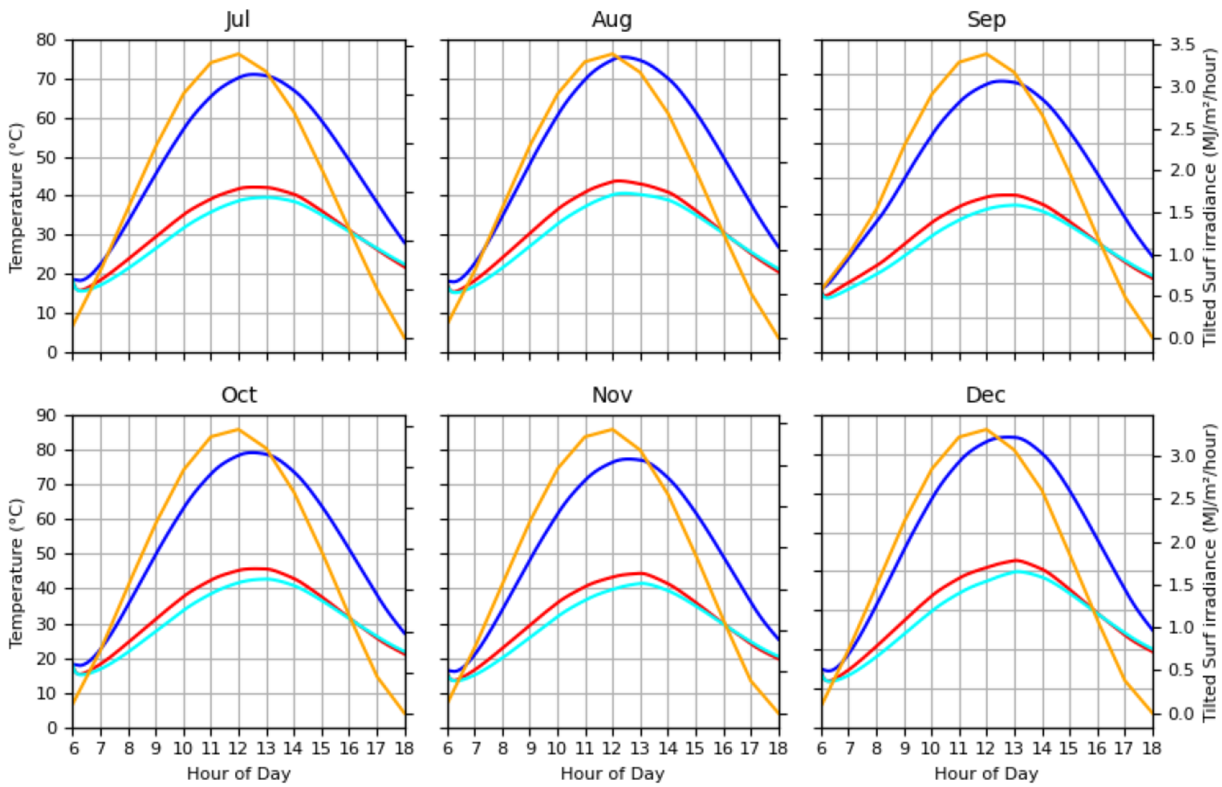

Figure 4: Comparison of glass cover temperature of single and double glass SAH

4.4. Air Stream Temperature

Figure 5 demonstrates superior performance of double-glass SAH, consistently achieving higher air temperatures than single-glass systems across all months, with air temperature peaking around midday and reaching 90.57°C in February. The temperature curve exhibits minimal thermal inertia, closely tracking solar radiation. The system exhibits prolonged heat retention greater than 80°C until 14:00 in most of the months. Whereas, the air temperature of the single-glass solar air heater exhibits reaches maximum of 82.34°C in February. This system maintains effective heating above 60°C between 10:00–14:00 in most months.

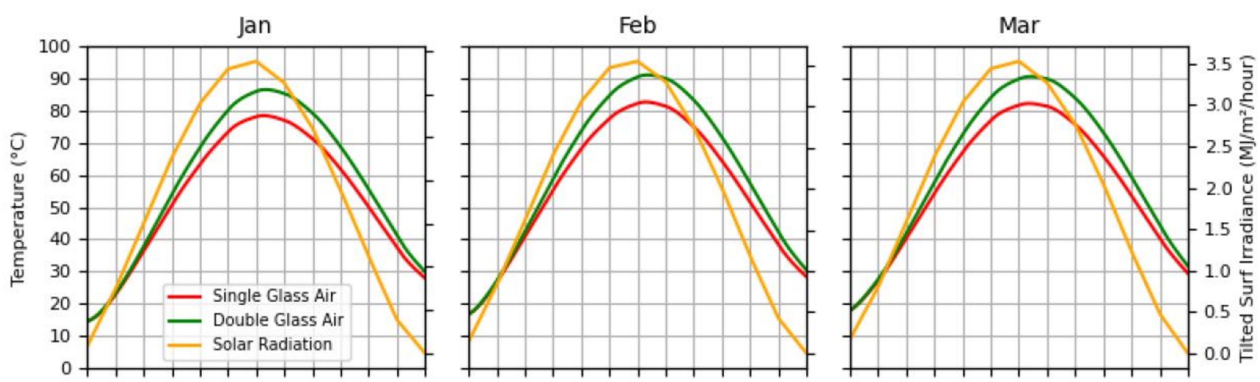

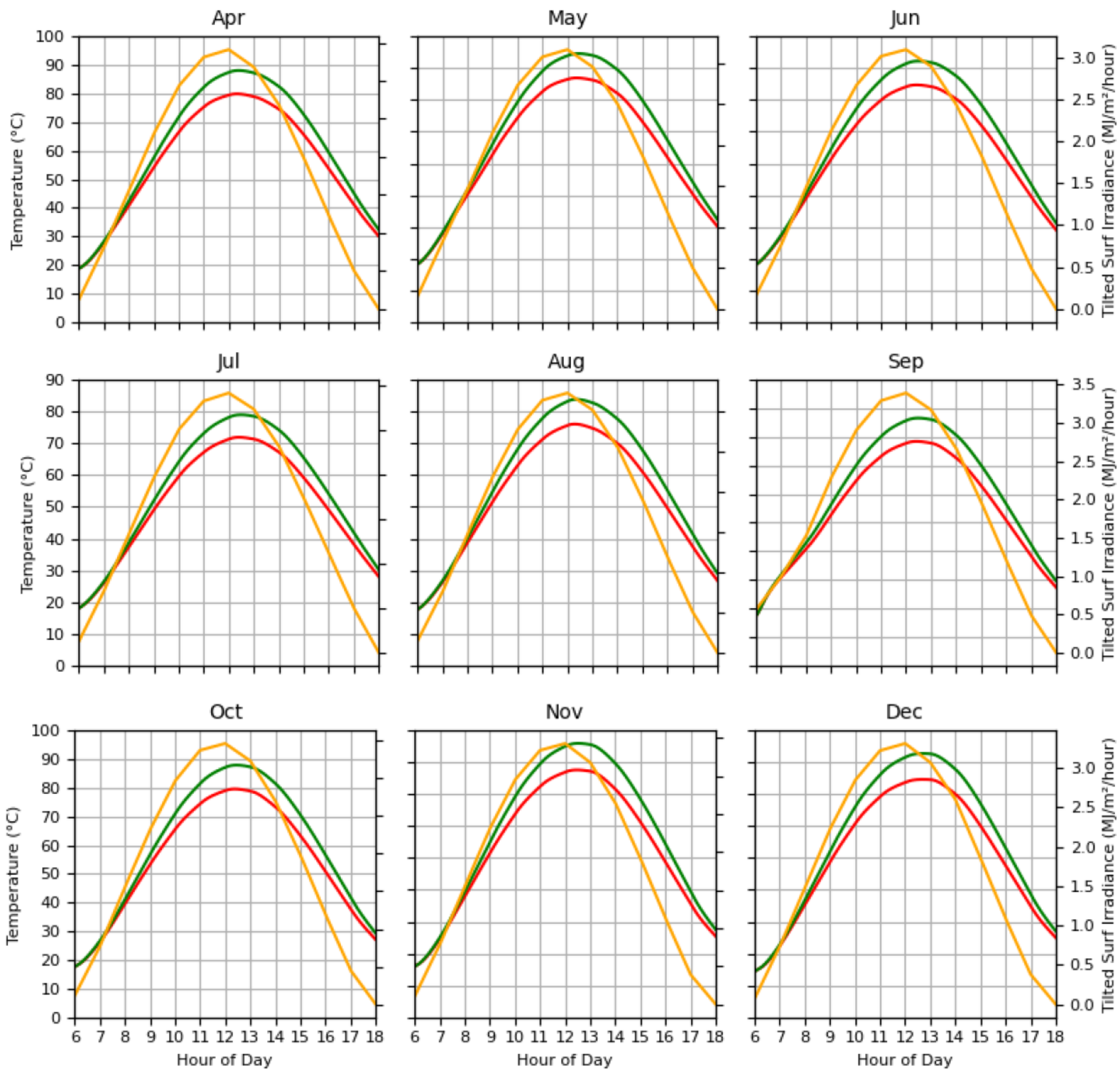

Figure 5: Comparison of air stream temperature of single and double glass SAH

The sustained heat conditions, shown in Figure 5, indicate strong potential for integration into textile industry drying processes, where consistent and elevated heat is essential for fabric treatment and moisture removal. Moreover, the extended duration of useful temperature ranges suggests that such systems could improve drying efficiency while reducing dependence on conventional energy sources in textile manufacturing. Furthermore, the double-glass configuration shows particularly significant advantages during peak solar hours of February and January, maintaining air temperatures 10°C higher than single-glass designs. Although both systems perform well when solar radiation is strongest, the maintained temperature differential between configurations underscores the double-glass system's superior energy efficiency and year-round reliability compared to single-pane alternatives.

5. CONCLUSION

In this paper, a comprehensive transient analysis of solar air heaters under specific weather conditions of Adama city, is conducted. The study aims to investigate transient thermal performance of single-glass and double-glass configurations by employing detailed energy balance of glass covers, absorber plate, and air stream. The analysis begins by predicting the solar radiation on a tilted surface. As such, it has been established that Adama city has peak global and beam radiation of 3.5 MJ/m²/hour, and 2.75 MJ/m²/hour in February, respectively. In addition, the single-glass SAH exhibits a consistent diurnal and seasonal pattern, with air temperatures peaking at 82.34°C in February, and maintaining effective heating above 60°C between 10:00–14:00 across most months. In contrast, the double-glass SAH reaches higher peak air temperatures of 90.57°C in February, with prolonged retention above 80°C until 14:00. The double-glass design maintains a 10°C higher air temperature advantage during peak solar hours compared to the single-glass system. Overall, both configurations effectively harness solar energy, but the double-glass SAH consistently outperforms the single-glass system, offering superior thermal performance across all operating conditions. Hence, the integration of SAHs into textile drying operations presents a sustainable and cost-effective alternative for supplying low-temperature thermal energy.

6. FUNDING STATEMENT

There is no fund received for this article.

7. DATA AVAILABILITY

The data supporting the findings of this study are accessible from the corresponding author.

8. CONFLICT OF INTEREST

The author states that there are no conflicts of interest to disclose.

REFERENCES

Adama City Admninistration (2025) *Adama - Geography*. Available at: https://cityadama.gov.et/en/city/ (Accessed: 18 March 2025).

Al-Chlaihawi, K.K.I., Alyas, B.H. and Badr, A.A. (2023) 'CFD Based Numerical Performance Assessment of a Solar Air Heater Duct Roughened by Transverse - Trapezoidal Sectioned Ribs', *International Journal of Heat and Technology*, 41(5), pp. 1273–1281. DOI:10.18280/ijht.410517.

Ameri, M., Farzan, H. and Nobari, M. (2021) 'Evaluation of Different Glazing Materials, Strategies, and Configurations in Flat Plate Collectors Using Glass and Acrylic Covers: An Experimental Assessment', *Iranian Journal of Energy and Environment*, 12(4), pp. 397–406. DOI:10.5829/ijee.2021.12.04.01.

Ansari, A.B. and Nassab, S.A. (2022) 'Numerical investigation on thermal performance enhancement of a flat-plate natural flow double-pass solar air heater – The effect of the absorber plate', *Energy Equipment and Systems*, 10(4), pp. 353–374.

Ashja, M. *et al.* (2025) 'Investigation of Performance Improvement in a Solar Air Heater Equipped with Impinging Jets: A Three-Dimensional Numerical Simulation', *Sustainable Energy and Artificial Intelligence*, 1(1), pp. 51–66. DOI:10.61186/seai.2410-1013.

Catarino, M.L., Sampaio, F. and Gonçalves, A.L. (2025) 'Sustainable Wet Processing Technologies for the Textile Industry: A Comprehensive Review', *Sustainability*, 17, pp. 1–33. DOI:10.3390/su17073041.

Čerdancova, L. *et al.* (2021) 'Energy Efficiency Benchmark in Textile Manufacturing Companies', *Environmental and Climate Technologies*, 25(1), pp. 331–342. DOI:10.2478/rtuect-2021-0024.

Climate Data (2024) *Adama Climate (Ethiopia)*. Available at: https://en.climate-data.org/africa/ethiopia/oromia/adama-2108/ (Accessed: 1 March 2025).

Duffie, J.A. and Beckman, W.A. (2013) *Solar Engineering of Thermal Processes*. Fourth Edi. Hoboken, New Jersey: John Wiley & Sons, Inc.

Farhana, K. *et al.* (2022) ‘Energy consumption, environmental impact, and implementation of renewable energy resources in global textile industries: an overview towards circularity and sustainability’, *Materials Circular Economy*, 4(15), pp. 1–16. DOI:10.1007/s42824-022-00059-1.

Farzan, H., Mahmoudi, M. and Zaim, E.H. (2023) ‘Thermal Analysis of New Solar Air Heater with Inclined Perforated Absorber Plates : Experimental Study’, *Iranian (Iranica) Journal of Energy & Environment*, 14(2), pp. 189–196. DOI:10.5829/ijee.2023.14.02.11.

Haldia, S. *et al.* (2024) ‘Numerical assessment of solar air heater performance having a broken arc and broken S-shaped ribs as roughness’, *Archives of Thermodynamics*, 45(1), pp. 23–31. DOI:10.24425/ather.2024.150435.

Khude, P. (2017) ‘A Review on Energy Management in Textile Industry’, *Innovative Energy & Research*, 6(2).

Kumar, L. *et al.* (2022) ‘Prospects and Challenges of Solar Thermal for Process Heating: A Comprehensive Review’, *Energies*, 15. DOI: 10.3390/en15228501.

Kumar, P. *et al.* (2022) ‘Economics of Implementing Solar Thermal Heating Systems in the Textile Industry’, *Energies*, 15, pp. 1–21. DOI:10.3390/en15124277.

Kumar, R. *et al.* (2024) ‘Thermal and effective assessment of solar thermal air collector with roughened absorber surface: An analytical examination’, *International Journal of Low-Carbon Technologies*, 19, pp. 1112–1123. DOI:10.1093/ijlct/ctae056.

Leseeka, L.C. (2024) *Integration of solar heating systems in the textile industry : A case study for Vishan Clothing Laundry*. National University of Lesotho.

Nemati, H. (2024) ‘Design, Simulation and Optimization of a Novel Transpired Tubular Solar Air Heater’, *Energies*, 17, pp. 1–24. DOI:10.3390/en17102323.

Patel, N.G. *et al.* (2021) ‘Energy model-based benchmarking of the drying process in the stenter machine’, *Drying Technology*, 39(8), pp. 1114–1133. DOI:10.1080/07373937.2021.1907401.

Ramaiah, R. and Shekar, K.S.S. (2018) ‘Solar Thermal Energy Utilization for Medium Temperature Industrial Process Heat Applications - A Review’, in *IOP Conf. Series: Materials Science and Engineering*. IOP Publishing. DOI:10.1088/1757-899X/376/1/012035.

Saboohi, Z. *et al.* (2023) ‘The effect of sinusoidal fins’ amplitude on the thermo-hydraulic performance of a solar air heater’, *Chemical Engineering Communications*, 210(5), pp. 773–787. DOI:10.1080/00986445.2022.2026338.

Shandal, J., Abed, Q.A. and Al-Shamkhee, D.M. (2020) ‘Simulation analysis of thermal performance of the solar air/water collector by using computational fluid dynamics’, *E3S Web of Conferences*, 180, pp. 1–10. DOI:10.1051/e3sconf/202018002015.

Singh, V.P. *et al.* (2022) ‘Recent Developments and Advancements in Solar Air Heaters: A Detailed Review’, *Sustainability*, 14, pp. 1–55. DOI:10.3390/su141912149.

Srivastava, R.K. and Rai, A.K. (2017) ‘A Review on Solar Air Heater Technology’, *International Journal of Mechanical Engineering and Technology*, 8(7), pp. 1122–1131. Available at: http://iaeme.com/Home/issue/IJMET?Volume=8&Issue=7.

Tasmin, N. *et al.* (2022) ‘Integration of Solar Process Heat in Industries: A Review’, *clean technologies*, 4, pp. 97–131. DOI:10.3390/cleantechnol4010008.

Venkatachalam, C., Samuel, G. and Solomon, G. (2019) ‘Dataset of solar energy potential assessment for Adama city (Ethiopia)’, *Data in brief*, 24, pp. 1–9. DOI:10.1016/j.dib.2019.103879.